Supplement to "Origin and Reduction of $1/f$ Magnetic Flux Noise in Superconducting Devices"

P. Kumar,[1] S. Sendelbach,[1,*] M. A. Beck,[1] J. W. Freeland,[2] Zhe Wang,[3,4] Hui Wang,[3,4] Clare C. Yu,[3] R. Q. Wu,[3] D. P. Pappas,[5] and R. McDermott[1,†]

[1] *Department of Physics, University of Wisconsin-Madison, Madison, Wisconsin 53706, USA*
[2] *Advanced Photon Source, Argonne National Laboratory, Argonne, Illinois 60439, USA*
[3] *Department of Physics and Astronomy, University of California, Irvine, California 92617, USA*
[4] *State Key Laboratory of Surface Physics and Key Laboratory for Computational Physical Sciences, Fudan University, Shanghai 200433, China*
[5] *National Institute of Standards and Technology, Boulder, Colorado 80305, USA*

(Dated: September 17, 2016)

This Supplement provides additional information on DFT calculations, Xray data, and flux noise measurements and analysis relevant to the results and conclusions presented in the main text. The document includes the following sections:

I. METHODOLOGY AND PARAMETERS OF DFT CALCULATIONS

Density functional theory (DFT) calculations were carried out using the highly-precise full potential linearized augmented plane-wave (FLAPW) method that has no shape approximation for charge, potential, and wave function expansions [1]. We used the generalized gradient approximation (GGA) in the formula of Perdew-Burke-Ernzerhof (PBE) for the description of the exchange-correlation interaction among electrons [2]. The core electrons were treated fully relativistically, while the spin-orbit coupling term for the valence states was invoked second variationally [3]. Energy cutoffs of 400 Ry and 25 Ry were chosen for the charge/potential and basis expansions in the interstitial region. In the muffin-tin region ($r_{\mathrm{Al}} = 2.00$ a.u. and $r_{\mathrm{O}} = 1.16$ a.u.), spherical harmonics with a maximum angular momentum quantum number of $l_{\max} = 8$ were used for all expansions. Electronic self-consistency was assumed when the root-mean-square differences between the input and output charge and spin densities were less than $1.0 \times 10^{-5}\ e/(\mathrm{a.u.})^3$. Numerical convergence of all physical properties against the number of k mesh points based on Monkhorst-Pack in the Brillouin zone (BZ) was carefully examined. Xray magnetic circular dichroism (XMCD) and Xray absorption spectra (XAS) were calculated according to the linear response equations elaborated in reference [3]. All DFT spectra were shifted upward in energy by 20 eV to compensate for the final state effect in the Xray absorption process. DFT results for O_2 adsorbed on Al_2O_3 (0001), with contributions from lattice oxygen atoms, are shown in Fig. S1.

* Present address: Northrop Grumman Corporation, Linthicum, Maryland 21203, USA
† Electronic address: rfmcdermott@wisc.edu

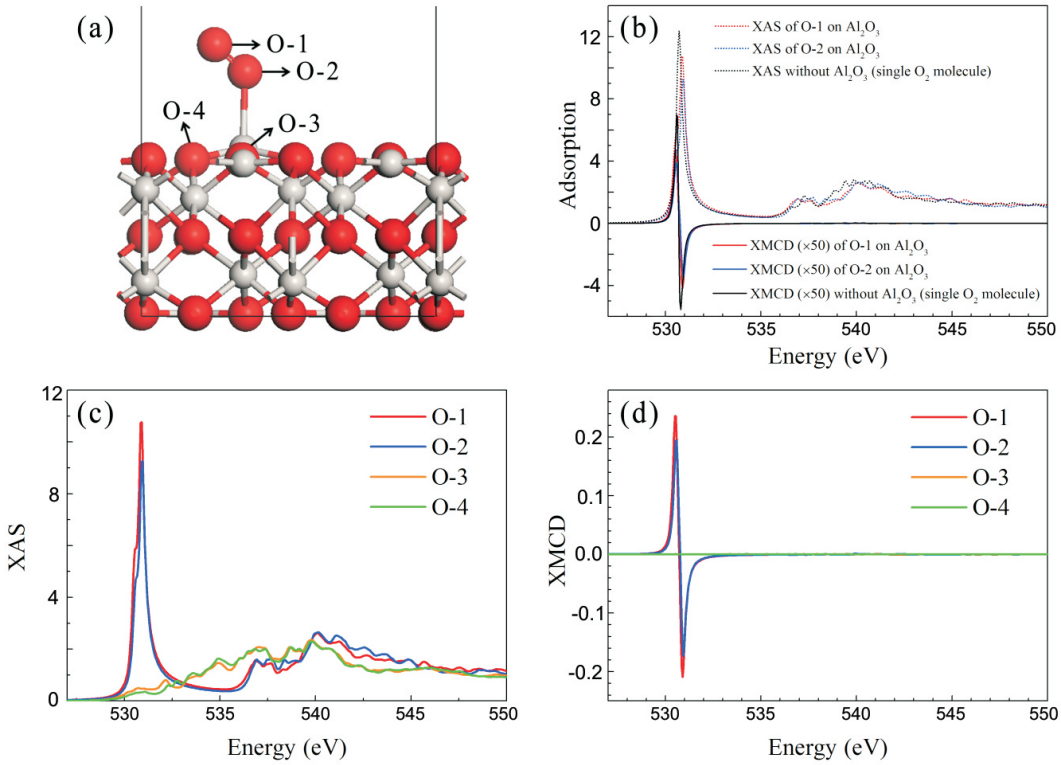

FIG. S1: (a) Schematic showing an O_2 molecule adsorbed on an Al_2O_3 (0001) surface. (b)-(d) DFT results for O_2/Al_2O_3, with contributions from O_2 and lattice oxygen atoms.

II. ADDITIONAL XAS AND XMCD DATA

In our initial set of experiments at the APS beamline, we examined the Al and O K-edges in Al films and the Nb L-edge and O K-edge in Nb films and observed no XMCD signal at any of these energies; see Fig. S2. For these measurements, the Al and the Nb thin film samples were cooled to the cryostat base temperature of 10 K in ultrahigh vacuum (UHV; $P < 10^{-9}$ Torr) conditions.

III. DEVICE FABRICATION

The aluminum first-stage SQUIDs were fabricated in the Wisconsin Center for Applied Microelectronics (WCAM) at the University of Wisconsin using a four layer process; a schematic of the device layer stack is shown in Fig. S3a, and the investigated geometries are shown in Fig. S3b. The aluminum base layer was deposited on an oxidized or nitrided silicon substrate by sputtering, and the layer was patterned and etched using Transene Etchant A. Next, a silicon nitride (SiN_x) or silicon oxide (SiO_x) wiring dielectric layer was grown by plasma enhanced chemical vapor deposition (PECVD). Vias were etched in the wiring dielectric using reactive ion etching (RIE) to define the Josephson junctions. An ion mill was used to remove the native oxide of the base layer, and the aluminum oxide of the tunnel barrier was formed by thermal oxidation in dry O_2. The Al counter electrode was deposited by sputtering, and the counter electrode traces were defined by a Transene wet etch. Finally, the Pd shunt resistors were formed by electron beam evaporation and liftoff. The junction areas were 2 μm^2, and the single-junction critical currents were in the range from 3-5 μA.

IV. MEASUREMENT SCHEME AND EXPERIMENTAL SETUP

Note on devices studied - The measurement of surface spin susceptibility requires us to controllably trap flux vortices in the thin films of our devices; see, [4]. While this is possible in our Nb-based SQUIDs, we have been unable to do this in our Al-based devices. Conversely, we are not able to perform careful measurements of flux noise in the

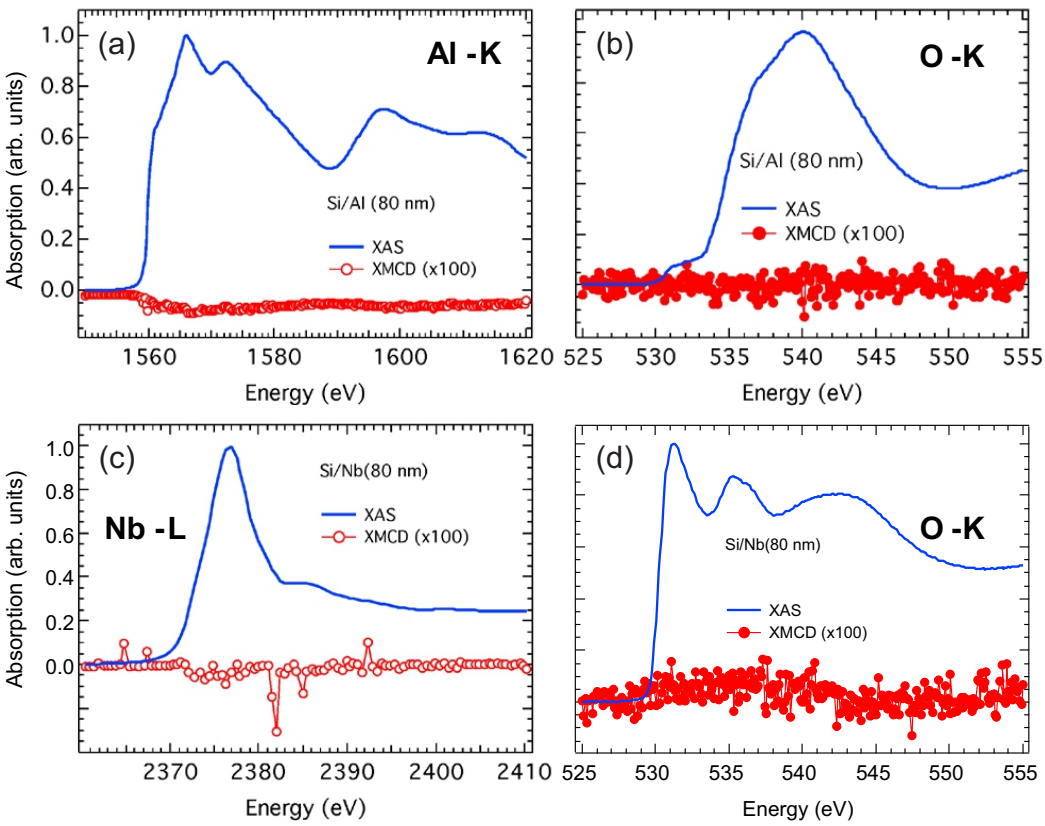

FIG. S2: XAS and XMCD data for (a) the Al K-edge and (b) the O K-edge in the Al thin film. XAS and XMCD data for (c) the Nb L-edge and (d) the O K-edge in the Nb thin film. No XMCD signal was observed at any of these energies.

Nb-based devices used to measure susceptibility, since resonant structure in the current-flux characteristics makes it impossible to stably voltage bias the devices as needed to perform the flux noise measurements. For these purely technical reasons, we were forced to characterize susceptibility in Nb-based devices and measure noise in Al-based devices. Nevertheless, the fact that the source of the flux noise is extrinsic to the fabrication materials means that even though the susceptibility and noise data are obtained on different materials, both results inform our understanding of flux noise.

Noise measurements - Flux noise measurements were performed on a series of Al-based SQUID devices. Devices were cooled to 100 mK in an adiabatic demagnetization refrigerator (ADR). The device under test was biased with a voltage, and fluctuating current through the device was measured by a second stage Nb-based SQUID incorporating an integrated multiturn input coil. In some cases, two second stage SQUIDs were used to simultaneously monitor the noise of the device under test, and the cross spectrum of the two measurement SQUIDs was used to suppress the added noise of the second stage. The measurement configurations are shown in Fig. S4a-b, and a block diagram of the experimental wiring is shown in Fig. S4c. Multiple layers of magnetic shielding were used to isolate the SQUIDs from ambient field fluctuations. The devices were protected from high-frequency interference by heavy filtering on the bias lines to the SQUIDs. All wires to the experimental stage incorporated copper powder filters (CPFs) at 3 K [5]. Additional inline *RC* filters were employed on the voltage- and flux-bias lines of the Al first-stage SQUID. Each second stage SQUID was operated in a flux-locked loop (FLL); the FLL output was passed through an anti-aliasing filter and digitized for further analysis. The flux noise power spectral density of the device under test was computed for each time series, and hundreds of such spectra were averaged together. We fit the averaged flux noise spectra to the functional form $S_\Phi(f) = A/f^\alpha + B$ to extract the noise power A and exponent α. A typical noise spectrum for an SiO_x-encapsulated device is shown in Fig. S4d along with the fit.

Grade 5 titanium enclosure - The noise measurements were conducted in a specially designed hermetic sample enclosure made from grade 5 titanium alloy (Ti-6Al-4V); see Fig. 2 in the main text. This alloy has excellent UHV

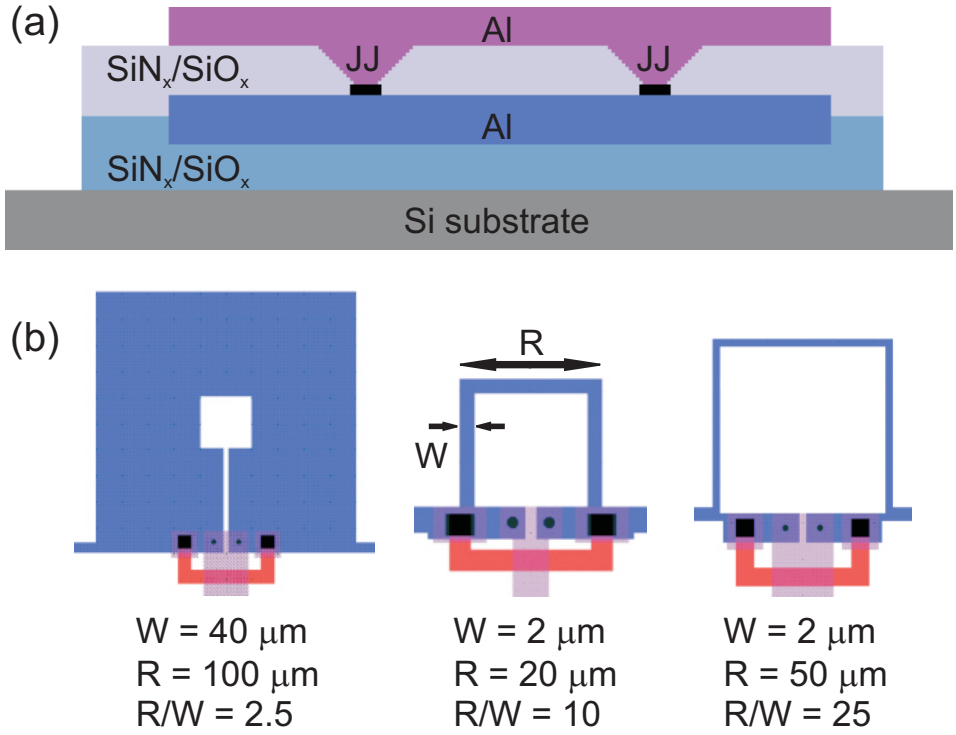

FIG. S3: (a) Sketch of Al SQUID layer stack. Upper dielectric: PECVD-grown SiN_x or SiO_x. Lower dielectric: thermal SiO_x or PECVD-grown SiN_x. (b) Device layouts showing different aspect ratios R/W used for investigation of dependence of flux noise on geometry. Here the base wiring is shown in blue, the counterelectrode is shown in pink, and the Pd normal metal shunts are shown in orange.

properties due to its low outgassing and its hardness, allowing realization of all-metal conflat seals. Moreover, the material is compatible with high-bandwidth weld-in hermetic SMA connectors, enabling both sensitive low-frequency measurements of flux noise and microwave-frequency control and readout needed for qubit experiments. Finally, grade 5 titanium superconducts at around 4.5 K, providing a magnetic shield for sensitive thin-film superconducting devices.

Experimental protocol for study of surface treatment - Devices were first mounted in the titanium enclosure and baseline data was collected: here, devices were not subjected to any surface modification and the titanium enclosure was not evacuated prior to installation in the ADR. In a subsequent cooldown, the same device was remeasured following improvement of the sample vacuum environment and/or surface modification by NH_3 passivation or UV illumination. The vacuum treatment included bakeout at 120°C under vacuum for several days to achieve pressure at the ion pump around 10^{-9} Torr. The UV-treated samples were irradiated under vacuum with a UV LED (300 mW at 365 nm); the UV LED was mounted on the conflat gasket a few millimeters from the sample using UHV-compatible epoxy. In some cases, a nonevaporable getter (NEG) pill (SAES Inc.) was activated in a separate chamber and transferred into the sample enclosure under vacuum prior to pinchoff of the vacuum cell. The NEG pill provides continuous pumping in the sample cell following pinchoff. In the case of NH_3 passivation, the titanium enclosure was first baked and evacuated until UHV conditions were reached; the cell was subsequently backfilled with 100 Torr of NH_3 before pinchoff. Flux noise power spectra of the surface treated devices were measured and compared to the baseline data.

V. DEPENDENCE OF NOISE ON DEVICE ASPECT RATIO

We observe a clear dependence of SQUID flux noise power spectral density on the aspect ratio of the SQUID loop, i.e., the ratio of loop width R to trace width W. This can be understood simply from reciprocity: the coupling of individual spins to the SQUID loop is proportional to the surface magnetic field at the spin location due to a test current that is injected in the SQUID loop [6–8]. The investigated geometries are shown Fig. S3b. We expect that

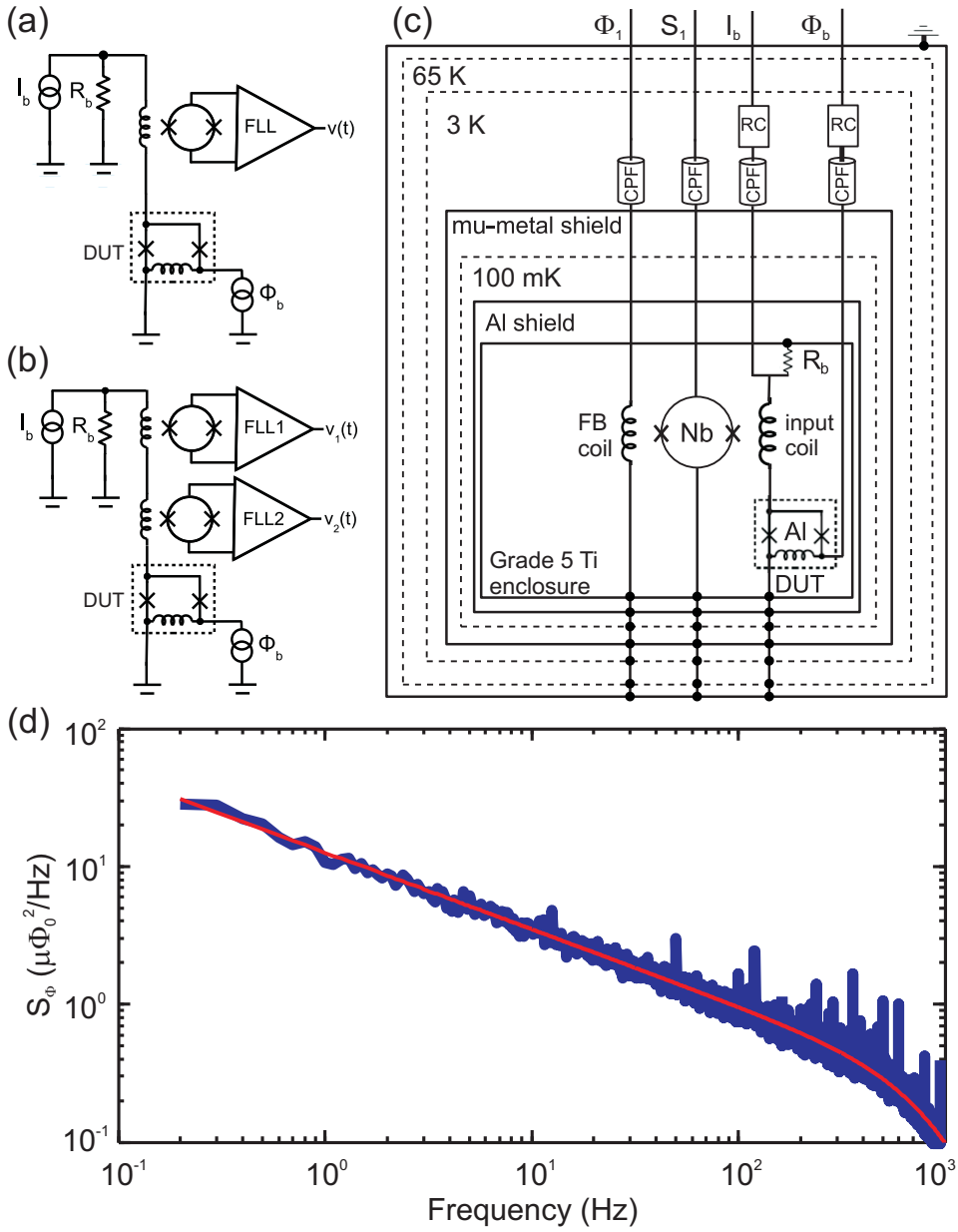

FIG. S4: Experimental setup and measurement scheme. (a) SQUID amplifier circuit. The Al-based device under test (DUT) is voltage biased and the external flux bias (Φ_b) is tuned to the point of maximum transfer function $dI/d\Phi$; current through the DUT is read out by a second-stage Nb-based SQUID, which is operated in flux locked loop (FLL). (b) Cross-correlation amplifier circuit. (c) Block diagram of measurement wiring in the ADR. The Nb and Al SQUIDs are housed in a grade 5 titanium enclosure and mounted at the cold stage of the ADR. The devices are protected from stray magnetic fields by two layers of superconducting shields (the grade 5 titanium enclosure itself, with $T_c \sim 4.5$ K, and a second stage of aluminum shielding, with $T_c \sim 1.2$ K) and by a single layer of cryogenic mu-metal. All bias lines are filtered with copper powder filters (CPF) at the 3 K stage. Additional RC filters are used for the bias lines (I_b and Φ_b) of the DUT at the 3 K stage. (d) Example noise spectrum of an SiO_x-encapsulated Al SQUID showing fit to the spectrum (red line).

flux noise power spectral density should scale linearly with R/W, apart from log corrections. In Fig. S5a we show flux noise power spectra of three SiO_x-encapsulated devices cofabricated on a single wafer; the expected scaling of noise power with aspect ratio is clearly seen. In Fig. S5b, we plot the flux noise power spectral density versus aspect ratio for a range of devices fabricated on 8 different wafers and incorporating both SiO_x and SiN_x encapsulation. For devices cofabricated on a single wafer, the linear scaling of flux noise with aspect ratio is clearly seen (red and blue

Device	Meas. Period 2012-2013 S_Φ(1 Hz) ($\mu\Phi_0^2$/Hz)	α	Meas. Period 2015-2016 S_Φ(1 Hz) ($\mu\Phi_0^2$/Hz)	α	Treatment	Post-treatment S_Φ(1 Hz) ($\mu\Phi_0^2$/Hz)	α
SiN_x-1	1.4	1.1	2.0	1.0	UHV	1.4	1.1
SiN_x-2	1.7	0.8	4.4	0.7	NH_3	2.4	0.7
SiN_x-3	1.6	0.9	2.8	1.0	UHV,UV	1.3	0.9
SiN_x-4	1.7	1.2	8.2	1.2	NH_3 UHV, UV	1.6 4.2	1.1 0.8
SiN_x-5	1.6	0.8	4.1	0.8	NH_3 UHV, UV	1.7 1.1	0.7 0.6
SiN_x-6	1.1	0.7	1.7	1.0	NH_3 UHV, UV	1.1 0.35	0.9 0.6
SiO_x-1	7.9	0.8	13.4	0.5	UHV,UV	13.7	0.5
SiO_x-2	7.5	0.7	6.5	1.0	UHV,UV	2.5	0.9
SiO_x-3	3.0	0.8	4.8	0.7	UHV,UV	5.1	1.1
SiO_x-4	2.9	1.3	3.0	0.8	UHV,UV	5.4	0.8

Table SI: Flux noise power spectral density S_Φ(1 Hz) and noise exponent α for the SiN_x- and SiO_x-encapsulated devices described in the main text in the period immediately following fabrication and in the before/after tests of surface treatment. The noise of the SiN_x-encapsulated devices increased significantly in the years between fabrication and the surface treatment studies.

dashed lines). In Fig. S5c, we show the dependence of flux noise exponent α on aspect ratio. No clear dependence is seen.

VI. DEPENDENCE OF NOISE ON DIELECTRIC ENCAPSULATION

Our measurements of the $1/f$ magnetic flux noise in these SQUIDs show a clear dependence of the noise power on the materials used to encapsulate the device loop, even in the absence of surface treatment. The data in Fig. S5b-c are from devices encapsulated in SiO_x (blue points) and in SiN_x (red points). We see significantly lower noise in the SiN_x-encapsulated devices, although the wafer-to-wafer variation in the noise from SiO_x-encapsulated devices is large, and some oxide-encapsulated devices show noise comparable to nitride-encapsulated devices. Preliminary results of our DFT calculations indicate there may be a high energetic barrier to reorientation of the O_2 magnetic moment when the molecule is adsorbed on a nitride-based surface as opposed to an oxide-based surface. Thus, adsorbed O_2 remains magnetically active down to millikelvin temperatures on an oxide surface, whereas the magnetic moment of O_2 starts to freeze out at higher temperatures on a nitride surface, leading to a reduction in noise.

VII. DEVICE AGING

The devices described in this manuscript were fabricated in 2012-2013. The study of the impact of device aspect ratio on noise was performed during that same interval; however, investigation of the effect of surface treatment was performed much later, in the time frame 2015-2016. Devices were not stored in a dry box or in a controlled environment. We find that the noise of the nitride-encapsulated devices increased significantly in the years following fabrication and prior to the study of surface treatment, suggesting a slow aging of the disordered device surface or a long timescale for the adsorption of strongly-bound magnetic species at 300 K. While we have no information about the evolution of the microscopic morphology of the disordered surfaces, we see that the NH_3-treated devices return to levels of flux noise that are comparable to those measured on the as-made devices, while the noise levels of the UHV/UV treated devices are in some cases significantly lower than those of the as-made devices (in one case by more than a factor of three). In all cases, the nitride devices showed significant noise reduction in the controlled before/after surface treatment studies described in the main text. Results are shown in Table SI.

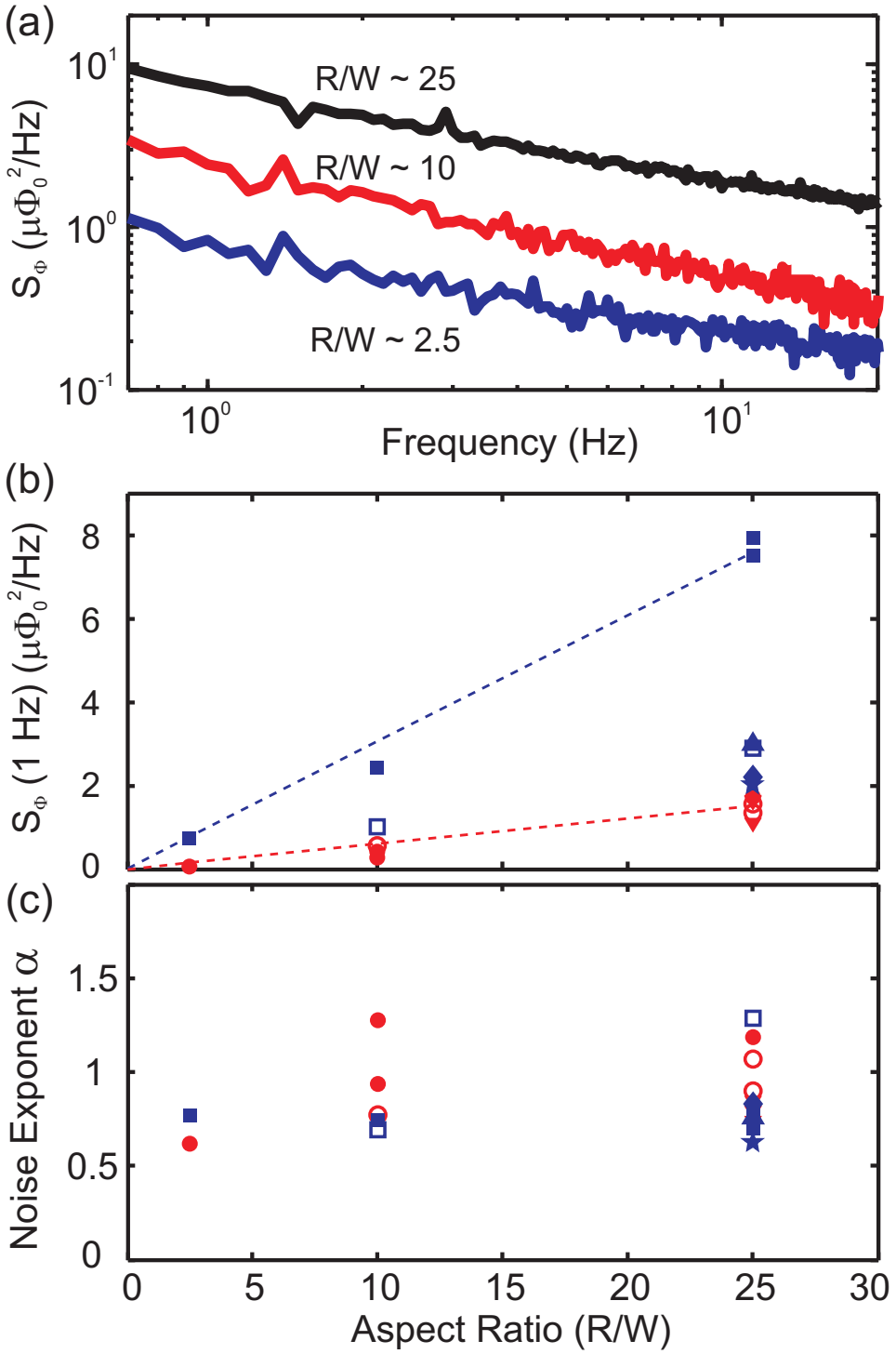

FIG. S5: Dependence of noise power spectral density on device aspect ratio and dielectric encapsulation. (a) Flux noise power spectra of three SiO_x-encapsulated devices with aspect ratio $R/W = 2.5$, 10, and 25; the linear scaling of noise power with device aspect ratio is clearly seen. (b) Dependence of flux noise power spectral density $S_\Phi(1\text{ Hz})$ on aspect ratio. The data span 8 different wafers incorporating both SiO_x (blue points) and SiN_x (red points) dielectric encapsulation. For devices cofabricated on a single wafer (indicated by identical symbols), the linear scaling of flux noise with aspect ratio is clearly seen (blue and red dashed lines). (c) Flux noise exponent α versus aspect ratio; no clear dependence is seen.

VIII. RUN-TO-RUN VARIATION OF MEASUREMENT RESULTS

In a typical measurement cycle, devices were characterized multiple times in an ADR at 100 mK, with repeated thermal cycles to 3 K between measurement runs in order to re-charge the ADR magnet. We observe 10% scatter in the flux noise power spectral density A and 29% scatter in the noise exponent α from run to run following thermal cycle to 3 K. In three cases, we re-measured devices following thermal cycle to 300 K and exposure of the device to atmosphere prior to the second cooldown. For these cases, we observe 7% variation in the noise power spectral density and 13% variation in the noise exponent. In Fig. S6a-b, we present data on the run-to-run variation in device noise. The robustness of the flux noise power spectral density suggests to us that fixed disorder at the surface dictates the adsorption and fluctuation dynamics of the O_2 spins. For comparison, in Fig. S6c-d we show the same before/after data for devices subjected to surface treatment. As discussed in the main text, we observe a significant noise suppression in nitride-encapsulated devices subjected to the various surface treatments, far beyond the typical run-to-run variation of the measurement. The average noise suppression observed in surface-treated nitride samples is ~ 2.8 times, with a maximum noise suppression factor of ~ 5.1. (All data shown in this figure are from high aspect ratio devices, $R/W = 25$).

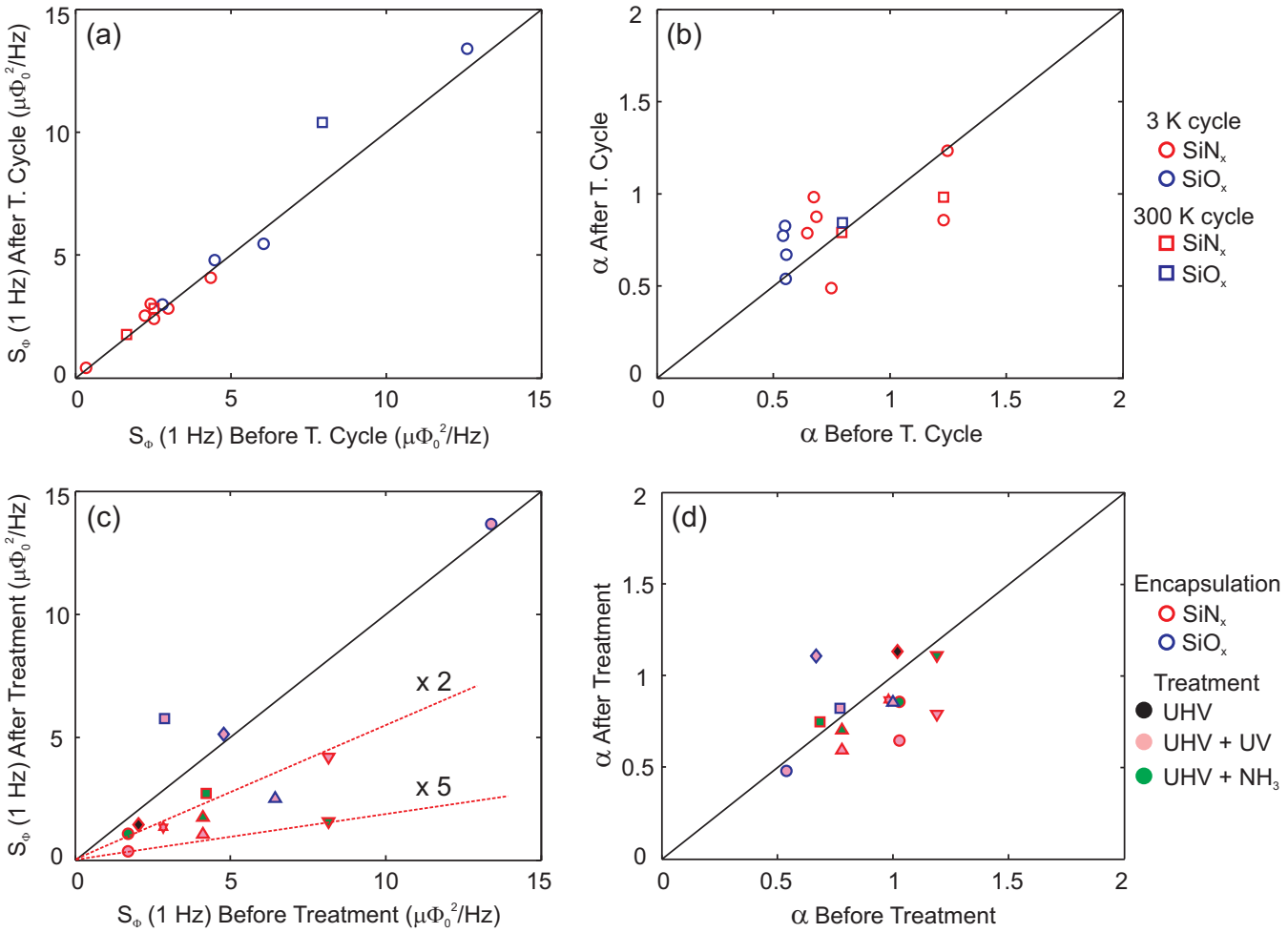

FIG. S6: (a) Flux noise power spectral density $S_\Phi(1\text{ Hz})$ and (b) noise exponent α before and after thermal cycle to 3 K and 300 K, without surface treatment. Blue points correspond to SiO_x-encapsulated devices, and red points correspond to SiN_x-encapsulated devices. (c)-(d) Analogous before/after plots of $S_\Phi(1\text{ Hz})$ and α for devices subjected to various surface treatments. Here, the blue border corresponds to SiO_x encapsulation, the red border corresponds to SiN_x encapsulation, and the fill color identifies the surface treatment (black: UHV alone; pink: UHV+UV; green: UHV+NH_3). An average reduction of ~ 2.8 in noise power spectral density is seen, with maximum noise suppression of 5.1. The red dashed lines in (c) correspond to noise suppression by a factor of 2 and 5.

[1] E. Wimmer, H. Krakauer, M. Weinert, and A. Freeman, Full-potential self-consistent linearized-augmented-plane-wave method for calculating the electronic structure of molecules and surfaces: O_2 molecule, Phys. Rev. B **24**, 864 (1981).

[2] J. P. Perdew, K. Burke, and M. Ernzerhof, Generalized gradient approximation made simple, Phys. Rev. Lett. **77**, 3865 (1996).

[3] R. Q. Wu and A. Freeman, Spin-orbit induced magnetic phenomena in bulk metals and their surfaces and interfaces, J. Magn. Magn. Mater. **200**, 498 (1999).

[4] S. Sendelbach, D. Hover, A. Kittel, M. Mück, J. M. Martinis, and R. McDermott, Magnetism in SQUIDs at millikelvin temperatures, Phys. Rev. Lett. **100**, 227006 (2008).

[5] J. M. Martinis, Ph.D. thesis, University of California, Berkeley (1985).

[6] R. C. Bialczak, R. McDermott, M. Ansmann, M. Hofheinz, N. Katz, E. Lucero, M. Neeley, A. D. O'Connell, H. Wang, A. N. Cleland, and J. M. Martinis, $1/f$ flux noise in Josephson phase qubits, Phys. Rev. Lett. **99**, 187006 (2007).

[7] S. M. Anton, J. S. Birenbaum, S. R. O'Kelley, V. Bolkhovsky, D. A. Braje, G. Fitch, M. Neeley, G. C. Hilton, H.-M. Cho, K. D. Irwin, F. C. Wellstood, W. D. Oliver, A. Shnirman, and J. Clarke, Magnetic flux noise in dc SQUIDs: Temperature and geometry dependence, Phys. Rev. Lett. **110**, 147002 (2013).

[8] S. LaForest and R. de Sousa, Flux-vector model of spin noise in superconducting circuits: Electron versus nuclear spins and role of phase transition, Phys. Rev. B **92**, 054502 (2015).